

# Wave Induced Flow and Transport in Sediment Beds

Accepted for publication: *Journal of the American Water Resources Association*

Fawaz Habel<sup>1</sup> and Amvrossios C. Bagtzoglou<sup>2</sup>

<sup>1</sup>*Department of Civil Engineering & Engineering Mechanics*

*Columbia University*

*New York, NY 10027*

<sup>2</sup>*Department of Civil & Environmental Engineering*

*University of Connecticut*

*Storrs, CT 06269-2037*

## **Abstract**

The fate of contaminant in large water bodies is highly influenced by the transfer of flow and solutes across the water-sediment interface. In this paper, we present an analytical model where flow in both sediment bed and open channel is coupled at the interface through a boundary layer occupying the upper part of the sediment bed. The presence of this layer allows not only the capture of the inertia effects through a drag term in the generalized Darcy's equation, but also the specification of different soil parameters for the two porous regions. The flow is advective and driven by wave action along the water surface. The resulting system is solved for the pressure and flux in each sediment layer. The generated transport velocity fields are linked to a random walk particles simulation that is used to examine the trajectories of solute particles. Comparison of these trajectories against experimental tracer tests suggests a pattern very similar to the one attributed to the presence of surface mounds [Huettel *et al.*, 1996]. The results clearly show the significance of the boundary layer and the drag term for soil with high permeability and the impact of both the thickness of the boundary layer and the length of the gravity wave relative to the depth of the water channel on the transport and exchange across the interface. The paper also examines the sensitivity of the mass exchange to the permeability of the two porous regions.

## **Key Terms**

Ground Water Hydrology, Modeling, Surface-Ground Water Interactions, Tracer Tests, Contaminants, Erosion/Sedimentation

## 1. Introduction

The fate and transport of contaminant in water bodies is controlled by the transfer of flow and solutes across the water-sediment interface. Different processes in both the water body and the sediment bed control the capture of solutes by the sediment bed and their subsequent release back into the water channel. Besides diffusional processes, field experiments in rivers point to the importance of convective transport in explaining the observed concentration profiles [*Musgrave and Reeburgh, 1982*].

In the case of gradient-driven flow, there is an extensive body of research work that was done to model and understand the fate of solutes in sediments and water channels. The classic approach to modeling the water-sediment interface has been the advective transport equation in the water channel with source/sink or first order linear terms to represent the exchange with the sediment bed. *Bencala* [1983] modeled the sorption mechanism while *Bencala and Walters* [1983] included terms for lateral inflows and transient storage. *Runkel et al.* [1996] extended both works and developed an equilibrium-based model that considered a variety of chemical processes. These models do not describe the mechanism of the exchange process but simply allow the model to reproduce the experimental/field results by fitting the exchange parameters.

In water of shallow depth and soil with high permeability, water waves could generate significant advective transport. *Riedl et al.* [1972] measured the total exchange due to the water flow across the sediment interface in the west Atlantic continental shelf while *Harrison et al.* [1983] estimated that mechanical dispersion induced by surface wave action can significantly increase the rate of solutes transport. *Savant et al.* [1987] modeled and measured experimentally the convective transport within sediment bed resulting from pressure variations on the sediment

surface. The sediment surface had stationary, triangular bed forms and the pressure was steady with a Darcy constitutive relationship between pressure and fluid velocities. Their results indicated that the interstitial flow driven by the pressure variations at the surface, often termed pumping, could dominate the transport of solutes within the sediment bed. *Shum* [1992] modeled the convective flow inside the sediment bed due to modulations along the water-sediment interface. The flow was modeled using Darcy's law and was driven at the surface by transversing water waves. He also measured the total exchange across the interface over one wave period and found net advective transport due to the non-elliptical pattern of pore water trajectories.

A different numerical and experimental approach, one that is based on the concept of Residence Time, was presented by *Elliott and Brooks* [1997a, b]. Their analysis focused on water movement driven by the presence of bed forms and on the mechanism of pumping, which is water flow induced by pressure, and turnover, which is water flow due to moving bed forms. They found pumping to be the main mechanism driving the flow and exchange in the lower parts of the bed whereas turnover was limited to the upper layer of the sediment bed. *Packman et al.* [2000a, b] extended the work of *Elliott and Brooks* [1997a, b] to colloid transport with stationary bed forms and finite sediment depth.

In all the work mentioned so far, the porous medium is assumed homogeneous and the flow in the sediment bed is described by Darcy's law. However, as pointed out by *Mendoza* [1988], the flow field within the sediment and the flow above it are strongly connected. The use of Darcy's law could be inappropriate in a narrow zone under-laying the water-sediment interface where inertia effects could be significant. Inherent in Darcy's law is the assumption that the convection

length per wave period is large compared with the pore spacing [Harrison *et al.*, 1983]. This imposes limitations on the range of parameters for which Darcy's law is applicable.

One focus of this paper is to study the impact of the inertial forces and the presence of the boundary layer on the exchange across the sediment interface. We present an analytical model where the flow in both the sediment bed and the channel is connected through a narrow boundary layer occupying the upper part of the sediment bed. A generalized Darcy's law describes the flow in this layer where inertia effects are captured through a drag term that allows departures from the linear dependence of specific flux on the head gradient. The presence of this layer also allows the specification of different soil parameters for the two porous regions. The driving force of the flow is the wave action along the water surface. In this work we use the term wave in a very general sense and refer to any periodic pressure disturbance due to a variety of physical processes, such as tidal effects near river mouths, flow over stationary or moving bed forms, surface wave action, etc. The resulting system is solved for the pressure and flux in each sediment layer. Another focus is to measure the trajectories of the contaminant as driven by the generated transport velocity (ratio of flux over porosity) fields induced by the imposed surface waves. This is achieved through a random walk simulation coupled with the transport velocity field obtained using the analytical model. Comparison of the trajectories of the solute particles against experimental tracer tests suggests a pattern very similar to the one attributed to the presence of surface mounds [Huettel *et al.*, 1996]. The paper also examines the sensitivity of the mass exchange to the thickness of the boundary layer, to the length of the gravity wave relative to the depth of the water channel, and to the permeability of the two porous regions.

## 2. Mathematical Model

The physical system is a two-dimensional domain with flow in the water channel assumed non-viscous and driven by wave motion along the water surface. The sediment bed is divided into two layers, each with its own soil characteristics. The flow through the porous medium is described by an extension of Darcy's law. The extension captures the inertial effects and was suggested by *Joseph et al.* [1982] through the inclusion of a drag term. Figure 1 shows a schematic description of the domain.

### 2.1. Flow Model

Potential flow theory is assumed valid in the river channel. The continuity equation is:

$$\nabla^2 \phi = 0 \quad h_2 \leq y \leq h_2 + h \quad (1)$$

where  $h$  varies around the mean water depth,  $h_1$ .

In the sediment bed, the equations of motion for both layer 2 (boundary layer) and layer 3 are:

$$-\nabla P_2 = \frac{\rho}{n_2} \frac{\partial \vec{q}_2}{\partial t} + \frac{\mu}{K_2} \vec{q}_2 + \frac{\rho c}{\sqrt{K_2}} |\vec{q}_2| \vec{q}_2 \quad h_3 \leq y \leq h_2 \quad (2)$$

$$-\nabla P_3 = \frac{\rho}{n_3} \frac{\partial \vec{q}_3}{\partial t} + \frac{\mu}{K_3} \vec{q}_3 + \frac{\rho c}{\sqrt{K_3}} |\vec{q}_3| \vec{q}_3 \quad 0 \leq y \leq h_3 \quad (3)$$

where  $\phi$  is potential,  $P$  is pressure head,  $q$  is flux,  $\rho$  is density,  $n$  is porosity,  $\mu$  is viscosity,  $K$  is permeability of the porous medium, and  $c$  is a non-dimensional coefficient that relates to the drag

due to the non-laminar flow near the interface with the surface water. When flow departs significantly from laminar the specific flux is no longer linearly related to the gradient of hydraulic head.  $c$  varies with the material and could range between 0.1 and 2.6 depending on the porosity [Joseph *et al.*, 1982]. Besides the inertial effects, the above two equations capture any stratification in the porous medium for both  $n$  and  $K$ .

The thickness of the boundary layer (zone two) is a very small fraction of the total thickness of the permeable bed. Accordingly, the variations in the flux along the vertical direction can be negligible and the magnitude term could be approximated with a constant average. In such case, the drag term is only captured as a constant input, estimated using the average flux in the boundary layer. For layer three, the inertial effects are usually insignificant and the drag term could be neglected. With such assumptions, equations (2) and (3) can be written as:

$$-\nabla P_2 = \frac{\rho}{n_2} \frac{\partial \bar{q}_2}{\partial t} + I_2 \bar{q}_2 \quad h_3 \leq y \leq h_2 \quad (4)$$

$$-\nabla P_3 = \frac{\rho}{n_3} \frac{\partial \bar{q}_3}{\partial t} + I_3 \bar{q}_3 \quad 0 \leq y \leq h_3 \quad (5)$$

with

$$I_2 = \frac{\mu}{K_2} + \frac{\rho c}{\sqrt{K_2}} |\bar{q}_2| \quad \text{and} \quad I_3 = \frac{\mu}{K_3} \quad (6a, b)$$

Using the continuity equation  $\frac{\partial(q_x)}{\partial x} + \frac{\partial(q_y)}{\partial y} = 0$  with (4) and (5), we obtain:

$$\nabla^2 P_2 = 0 \quad \text{and} \quad \nabla^2 P_3 = 0 \quad (7a,b)$$

In terms of boundary conditions, the domain is a two-dimensional space where the water flow is bounded above by a free water surface, below by the bed-water interface, and the porous bed has an impermeable lower bound. In the horizontal direction, the domain is assumed to span from one to multiple gravity-wavelengths ( $\chi$ ) implying the existence of periodic boundary conditions.

At the bottom of the porous medium, the vertical flux across this interface vanishes and, therefore, no transfer of momentum or pressure can take place. Accordingly, we impose a zero pressure gradient:

$$\frac{\partial P_2}{\partial y} = 0 \quad \text{at } y = 0 \quad (8)$$

At the interface, the continuity of pressure results into the following equation:

$$\rho \frac{\partial \phi}{\partial t} = P_2 \quad \text{at } y = h_2 \quad (9)$$

Equation (9) is only applicable for the case where fluid in the open channel flow has a zero viscosity. In the case of viscous fluid, a detailed derivation of the appropriate boundary condition can be found in *Murray [1965]*.

The other necessary boundary condition at the riverbed interface is the continuity of vertical discharge:

$$-\frac{\partial \phi}{\partial y} = q_y \quad \text{at } y = h_2 \quad (10)$$

As for the free surface boundary, the condition that the normal components of the fluid velocity at the free surface are equal to the normal velocity of the surface gives the following [Lamb, 1932]:

$$\frac{\partial \eta}{\partial t} = -\frac{\partial \phi}{\partial y} \quad \text{at } y = h \quad (11)$$

The water surface elevation will be assumed to be a simple harmonic function:

$$\eta = E \exp[i(kx - \omega t)] \quad (12)$$

in which  $E$  is a constant amplitude,  $k$  is the wave number of the wave, and  $\omega$  is the angular frequency of the gravity wave.

$$\omega = 2\pi/T ; \quad k = 2\pi/\chi \quad (13a, b)$$

$T$  being the period of the gravity wave, and  $\chi$  the wavelength.

At the interface between the two porous zones, continuity of pressure and flux is assumed in the vertical

$$P_3 = P_2 \quad \text{at } y = h_3 \quad (14)$$

$$q_{2y} = q_{3y} \quad \text{at } y = h_3 \quad (15)$$

## 2.2. Analytical solutions

Using separation of variables and applying appropriate boundary conditions, the solutions to equations (1) and (7a, b) are written as follows:

$$\phi = \text{Re}\{\exp[i(kx - \omega t)][A \cosh k(y - h_2) + B \sinh k(y - h_2)]\} \quad (16)$$

$$P_2 = \text{Re}\{\exp[i(kx - \omega t)][C \cosh k(y - h_3) + D \sinh k(y - h_3)]\} \quad (17)$$

$$P_3 = \text{Re}\{\exp[i(kx - \omega t)][J \cosh k(y) + L \sinh k(y)]\} \quad (18)$$

Constants  $A$ ,  $B$ ,  $C$ ,  $D$ , and  $J$  can be found in the appendix. Constant  $L$  is equal to zero. Solving for the real parts of the pressure fields in regions (2) and (3) one gets

$$P_2(x, y; t) = \frac{Ek\rho\omega^2}{4(D_{21} + D_{22})} (F_1(y) \cos(kx - \omega t) + F_2(y) \sin(kx - \omega t)) \quad (19)$$

$$P_3(x, y; t) = \frac{Ek\rho\omega^2}{D_{21} + D_{22}} \cosh(ky) (G_1 \cos(kx - \omega t) + G_2 \sin(kx - \omega t)) \quad (20)$$

Constants  $F_1(y)$ ,  $F_2(y)$ ,  $D_{21}$ ,  $D_{22}$ ,  $G_1$ , and  $G_2$  can be found in the appendix.

Differentiating (19) and (20) with respect to  $x$  and  $y$  and substituting into (4) and (5), we obtain four ODE equations that describe the fluxes in both zones. The solutions of the ODEs are [Tenenbaum and Pollard, 1985]:

$$q_{2x}(x, y; t) = \frac{Ek^2 n\rho\omega^2}{4(D_{21} + D_{22})(I_2^2 n^2 + \rho^2 \omega^2)} \left[ \begin{aligned} &(-F_2(y)I_2 n + F_1(y)\rho\omega) \cos(kx - \omega t) + \\ &(F_1(y)I_2 n + F_2(y)\rho\omega) \sin(kx - \omega t) \end{aligned} \right] \quad (21)$$

$$q_{2y}(x, y; t) = \frac{Ek^2 n \rho \omega^2}{4(D_{21} + D_{22})(I_2^2 n^2 + \rho^2 \omega^2)} \left[ \begin{array}{l} (S_1(y)I_2 n + S_2(y)\rho\omega) \cos(kx - \omega t) + \\ (S_2(y)I_2 n - S_1(y)\rho\omega) \sin(kx - \omega t) \end{array} \right] \quad (22)$$

$$q_{3x}(x, y; t) = \frac{Ek^2 n \rho \omega^2}{(D_{21} + D_{22})(I_2^2 n^2 + \rho^2 \omega^2)} \cosh(ky) \left[ \begin{array}{l} (-G_2 I_2 n + G_1 \rho \omega) \cos(kx - \omega t) + \\ (G_1 I_2 n + G_2 \rho \omega) \sin(kx - \omega t) \end{array} \right] \quad (23)$$

$$q_{3y}(x, y; t) = -\frac{Ek^2 n \rho \omega^2}{(D_{21} + D_{22})(I_2^2 n^2 + \rho^2 \omega^2)} \sinh(ky) \left[ \begin{array}{l} (G_1 I_2 n + G_2 \rho \omega) \cos(kx - \omega t) + \\ (G_2 I_2 n - G_1 \rho \omega) \sin(kx - \omega t) \end{array} \right] \quad (24)$$

Constants  $S_1(y)$  and  $S_2(y)$  can be found in the appendix.

### 2.2.1. Darcy's Flow Model

The case of Darcian flow in a homogeneous sediment bed is a simplified version of the model presented in 2.2. The analytical solutions for pressure and flux can be deduced from (19) – (20) by

noting that  $h_3 \rightarrow h_2$  and  $I_2 = I_3 = \frac{\mu}{K}$ .

$$P_2(x, y; t) = P_3(x, y; t) = \frac{2E\rho\omega^2 \cosh(ky) \left( \begin{array}{l} (I_2^2 n^2 + \rho^2 \omega^2) \cos(kx - \omega t) \cosh(kh_2) \\ \sinh(kh_1) + n\rho\omega \cosh(kh_1)(\rho\omega \cos(kx - \omega t) - \\ I_2 n \sin(kx - \omega t)) \sinh(kh_2) \end{array} \right)}{k \left( \begin{array}{l} 2(I_2^2 n^2 + \rho^2 \omega^2) \cosh(kh_2)^2 \sinh(kh_1)^2 + n\rho^2 \omega^2 \\ (2n \cosh(kh_1)^2 \sinh(kh_2)^2 + \sinh(2kh_1) \sinh(2kh_2)) \end{array} \right)} \quad (25)$$

$$q_{2x}(x, y; t) = q_{3x}(x, y; t) = \frac{-2E\rho\omega^2 \cosh(ky) \left( \begin{array}{l} (I_2^2 n^2 + \rho^2 \omega^2) \sin(-kx + \omega t) \cosh(kh_2) \\ \sinh(kh_1) + n\rho\omega \cosh(kh_1)(\rho\omega \sin(-kx + \omega t) - \\ I_2 n \cos(kx - \omega t)) \sinh(kh_2) \end{array} \right)}{I_2 \left( \begin{array}{l} 2(I_2^2 n^2 + \rho^2 \omega^2) \cosh(kh_2)^2 \sinh(kh_1)^2 + n\rho^2 \omega^2 \\ (2n \cosh(kh_1)^2 \sinh(kh_2)^2 + \sinh(2kh_1) \sinh(2kh_2)) \end{array} \right)} \quad (26)$$

$$q_{2y}(x, y; t) = q_{3y}(x, y; t) = \frac{-2E\rho\omega^2 \sinh(ky) \left( \begin{array}{l} (I_2^2 n^2 + \rho^2 \omega^2) \cos(kx - \omega t) \cosh(kh_2) \\ \sinh(kh_1) + n\rho\omega \cosh(kh_1)(\rho\omega \cos(kx - \omega t) - \\ I_2 n \sin(kx - \omega t)) \sinh(kh_2) \end{array} \right)}{I_2 \left( \begin{array}{l} 2(I_2^2 n^2 + \rho^2 \omega^2) \cosh(kh_2)^2 \sinh(kh_1)^2 + n\rho^2 \omega^2 \\ (2n \cosh(kh_1))^2 \sinh(kh_2)^2 + \sinh(2kh_1) \sinh(2kh_2) \end{array} \right)} \quad (27)$$

### 2.3. Mass transport

The magnitude of the total exchange across the water sediment interface depends on the flux across that interface and the strength of the wave motion. The flux of pore water per unit length is given by:

$$dF_y = u \frac{dy}{dl} + v \frac{dx}{dl} \quad (28)$$

Where  $dl$  is a unit length along the water-sediment interface. In the case of a flat bed, the flux across the interface per unit length becomes:

$$dF_y = q_y(x, h_2, t) \quad (29)$$

where  $q_y$  is given by (22). Integrating along a wave period for the total exchange, the transport per unit length is approximated by:

$$d\bar{F}_y = \int_0^T |dF| d\tau \quad (30)$$

The net flux over one wavelength is zero because the flow over one wave period is separated into two equal regions, one with inflow and the other with outflow. However, for mass transport in natural media caused by wave motion, it is important to measure the total flow across the sediment

interface since there may exist variations in soil characteristics. This flow varies with vertical distance but this work only focuses on the volume exchange at  $y = h_2$ . The effects of wave and soil characteristics on the net flow, namely equation (30), are examined in the analysis section.

The approach for estimating mass transport across the water-bed interface described above has two assumptions embedded in it: (1) The contaminant is uniformly distributed in a layer below the riverbed interface (as opposed to over a finite area) such as the total amount of solute transported across the interface is directly proportional to the flux, and (2) once a solute particle enters the sediment bed, it remains there without the possibility that it finds its way back into the water surface.

#### 2.4. Random walk transport

A numerical approach to study mass transport under an imposed transport velocity field is the “particle method”, whereby the mass of solute is represented by a large number of discrete particles that represent the solute distributed in space. Each particle has a set of attributes such as mass and position, and in groundwater problems, the trajectory of each particle is simulated. One of the most widely used simulation methods is based on the random walk approach, which is a formulation of the Brownian motion. In terms of position, the motion of a particle is modeled as:

$$\frac{dX}{dt} = d(X, t) + ra(X, t) \cdot \xi(t) \quad (31)$$

where the last term is a random factor. Following many transformations [Bagtzoglou et al., 1991], the previous equation can be written as a discrete *Ito* stochastic differential equation:

$$X^{n+1} = X^n + d(X, t)\Delta t + ra(X, t) \cdot W(t) \quad (32)$$

$W(t)$  is a random variable given by  $Z\sqrt{\Delta t}$  where  $Z$  is a random number with zero mean and unit variance. Equation (32) allows the transport of particles over a number of time steps. A more detailed description of the random walk approach can be found in *Bagtzoglou et al. [1991, 1992]*.

Concerning the initial and boundary conditions, the solute is simulated by introducing a number of particles at specific nodes, and no-flux boundaries are treated as reflection planes where the particles bounce back and stay within the domain. Periodic boundary conditions, whereby a particle escaping to the left is re-introduced at the right boundary have also been explored. At the riverbed interface, once a particle crosses the domain, zero mass is assigned to it so that it is effectively removed from the computations.

This approach provides an easy and simple way of simulating solute transport subject to the wave driven advective flow. The impact of both soil and wave characteristics can be easily assessed and solute trajectories are visualized and compared against experimental or field studies. Our random walk simulation results were obtained for pure advective solute transport.

### **3. Analysis and discussion**

In this section, we first compare the above model with an already derived analytical solution. The comparison provides a check of the model's validity within the limits of this specific test. In the second part, the flow and transport problems are addressed. The impact of the soil and wave characteristics on the mass transfer across the sediment interface is investigated. Also, the solute

trajectories subject the water wave motion are simulated and qualitatively compared to experimental tests.

### 3.1. Comparison with an analytical solution

To test the mathematical model, a comparison with an analytical solution for the pore pressure is carried out. *Gu and Wang* [1991] have presented an analytical solution for the pore pressure in a uniform porous medium with unsteady linear flow:

$$P(x, y; t) = D \exp[i(kx - wt)] \cosh[ky] \quad (33)$$

$$D = \frac{\rho g E}{\cosh[kh_1] \cosh[kh_2] - (i/f_0) \sinh[kh_1] \sinh[kh_2]} \quad (34)$$

$f_0$  is a linearized resistance coefficient equivalent to  $\frac{\mu}{K\rho w}$ . Figure 2 shows the comparison between the real part of (33) and (34) and the solution presented in section 2.2.1. The input parameters are listed in Table 1. Since the solution of *Gu and Wang* [1991] is for a homogeneous porous medium, it should be noted that this comparison serves only as a limiting case verification of our model.

#### 3.2.1 Model sensitivity to wave, domain, and soil characteristics

In order to study the sensitivity of the model, a parametric study was conducted by changing various characteristics of the wave, domain geometry, and soil. A summary of the parameters used in the sensitivity analysis is presented in Table 2. The net exchange across the sediment interface over one wave period is zero. The cyclic nature of the wave motion results in an

upward vertical flow over half the wavelength and downward vertical flow over the other half. Figure 3 shows the velocity underneath the water wave as it travels from the left towards the right of the domain as indicated in Figure 1. Therefore, the three plots of Figure 3 can be viewed as either the variation of transport velocity (or flux for the case of uniform porosity) with vertical distance at three distinct horizontal locations and at the same time or at one location at three different times. For the case studied here (input parameters are listed in Table 2), downward vertical velocity occupies the middle half of the wave domain. The total, instead of the net, exchange is measured in this section in order to study the effects of wave, domain, and soil characteristics. We will examine the impact of both the thickness of the boundary layer and the length of the gravity wave relative to the depth of the water channel on the transport and exchange across the interface. We will also assess the significance of stratification in the soil permeability on the exchange.

For sediment with low permeability, *Harrison et al.* [1983] showed the little impact surface wave action and the resulting advection could have on the rate of solute transport into a sandy seabed. Since the inertial forces in the boundary layer are insignificant for weak advective transport, it is expected that the impact of non-linear flow on mass transfer is negligible for sediments with low permeability. Figure 4 confirms this result by plotting the variation of the flux as a function of the ratio of the thickness of layer three relative to the total thickness of the sediment bed  $R = h_3/h_2$ . With the ratio being equal to one corresponding to linear flow in a homogeneous sediment bed, the presence of the boundary layer affects the flux across the riverbed interface only for the case of high permeability.

Defining  $S$  as the ratio of the wavelength to the mean depth of the water channel,  $S = \chi/h_1$ , the mass exchange across the riverbed interface is sensitive to this ratio especially for sediment beds with high permeability. To better illustrate the point, Figure 5 plots the variation of the flux with  $S$  for three different permeabilities. The increase in flux with increase in  $S$  seems to reach an asymptotic level that is dependent on permeability. This is due to the fact that after a certain point, the increase in wavelength has little impact on the pressure field over the sediment bed. For low permeability, the analysis confirms the expectation of a low mass-exchange. As far as the soil characteristics are concerned, the impact of stratification along the sediment thickness is only significant for high permeability soils. Assuming that permeability in the boundary layer varies between 20% and 100% of that in the remaining sediment bed, Figure 6 shows the little impact the ratio  $K_2/K_3$  has on the exchange for soil with low permeability (for values of the ratio between 0.5 and 1). For high permeability, the flux appears to be linearly depending on the ratio  $K_2/K_3$ , which is a reasonable outcome given that for values of  $K_2 \leq K_3$  the boundary layer acts as a barrier to flow across the riverbed interface. Varying this ratio with the thickness of the boundary layer (Figure 7) we conclude that the exchange across the riverbed interface is much more influenced by the ratio of soil permeabilities for thin boundary layers. Note that the ratio  $R=1$  is an asymptotic value, which was approached with a 0.0001 accuracy. At the other end of the spectrum, namely for relatively thick boundary layers, the ratio of soil permeabilities is less significant in regards to the flux across the riverbed interface. Again, this is considered reasonable since for thick boundary layers the exchange at the riverbed interface is influenced very little by changes in the permeability of the deep sediment bed.

### 3.2.2 *Random walk simulations*

In this section, we will focus on the trajectories of solute particles under the generated transport velocity fields. We will simulate the transport of solute particles and compare their trajectories against experimental studies that visualized the vertical solute transport in sediment beds.

Figure 8 shows the distribution of solute particles before and during the simulation. Initially, the solute is distributed into a horizontal sediment layer located in the middle of the sediment bed (Figure 8a). With the random walk simulation, the solute particles are redistributed in an inverted half arc shape that extends to the surface of the porous bed (Figure 8b). This trajectory is very similar to the trajectory recorded in an experimental study by *Huettel et al.* [1996, Experiment 2] as presented in adapted form in Figure 9. These two observations confirm that the model described in this paper could accurately describe the contaminant transport in the sediment bed and across the interface for sediments with high permeability and for relatively a shallow water channel.

## **4. Conclusions**

In this paper, we presented an analytical model where flow in both sediment bed and open channel is coupled at the interface through a boundary layer occupying the upper part of the sediment bed. The advective flow is driven by wave action along the water surface. The resulting system is solved for the pressure and flux in each sediment layer and the generated transport velocity fields are linked to a random walk particle simulation that is used to examine the trajectories of solute particles. The results show the significance of the non-linear flow for soil with high permeability and the impact of both the thickness of the non-linear domain and the length of the gravity wave

relative to the depth of the water channel on the transport and exchange across the interface. Also, comparison of the simulated trajectories against experimental tracer tests suggests a pattern very similar to the one attributed to the presence of surface mounds. Further extensions of this model point to the need to move away from the flat bed assumption and to include the effects of rippled sediment interface.

## Appendix: Constants for the Analytical Solutions

### Pore Pressure

$$A = \frac{E\omega(iI_2n + \rho\omega)[(-n(I_2 + I_3) - 2i\rho\omega)\cosh kh_2 + n(I_2 + I_3)\cosh(k(h_2 - 2h_3))]}{2k \left[ \begin{array}{l} (iI_2n + \rho\omega)\cosh k(h_2 - h_3)[(iI_3n + \rho\omega)\cosh(kh_3)\sinh(kh_1) + \\ n\rho\omega\cosh(kh_1)\sinh(kh_3)] + \sinh k(h_2 - h_3)[n\rho\omega(iI_3n + \rho\omega)\cosh(kh_1) \\ \cosh(kh_3) + (iI_2n + \rho\omega)^2\sinh(kh_1)\sinh(kh_3)] \end{array} \right]} \quad (A1)$$

$$B = \frac{En\rho\omega^2 \left[ \begin{array}{l} (iI_3n + \rho\omega)\cosh(kh_3)\sinh k(h_2 - h_3) + \\ (iI_2n + \rho\omega)\cosh(k(h_2 - h_3))\sinh(kh_3) \end{array} \right]}{\left[ \begin{array}{l} (I_2n - i\rho\omega)\cosh k(h_2 - h_3)[(iI_3n + \rho\omega)\cosh(kh_3)\sinh(kh_1) + \\ n\rho\omega\cosh(kh_1)\sinh(kh_3)] + \sinh k(h_2 - h_3)[n\rho\omega(I_3n - i\rho\omega) \\ \cosh(kh_1)\cosh(kh_3) + i(I_2n - i\rho\omega)^2\sinh(kh_1)\sinh(kh_3)] \end{array} \right]} \quad (A2)$$

$$C = \frac{E\rho\omega^2(iI_2n + \rho\omega)(iI_3n + \rho\omega)\cosh(kh_3)}{k \left[ \begin{array}{l} (I_2n + \rho\omega)\cosh k(h_2 - h_3)[(iI_3n + \rho\omega)\cosh(kh_3)\sinh(kh_1) + \\ n\rho\omega\cosh(kh_1)\sinh(kh_3)] + \sinh k(h_2 - h_3)[n\rho\omega(iI_3n + \rho\omega) \\ \cosh(kh_1)\cosh(kh_3) + (iI_2n + \rho\omega)^2\sinh(kh_1)\sinh(kh_3)] \end{array} \right]} \quad (A3)$$

$$D = \frac{E\rho\omega^2(iI_2n + \rho\omega)^2\sinh(kh_3)}{k \left[ \begin{array}{l} (iI_2n + \rho\omega)\cosh k(h_2 - h_3)[(iI_3n + \rho\omega)\cosh(kh_3)\sinh(kh_1) + \\ n\rho\omega\cosh(kh_1)\sinh(kh_3)] + \sinh k(h_2 - h_3)[n\rho\omega(iI_3n + \rho\omega) \\ \cosh(kh_1)\cosh(kh_3) + (iI_2n + \rho\omega)^2\sinh(kh_1)\sinh(kh_3)] \end{array} \right]} \quad (A4)$$

$$J = \frac{E\rho\omega^2(iI_2n + \rho\omega)(iI_3n + \rho\omega)}{k \left[ \begin{array}{l} (iI_2n + \rho\omega)\cosh k(h_2 - h_3)[(iI_3n + \rho\omega)\cosh(kh_3)\sinh(kh_1) + \\ n\rho\omega\cosh(kh_1)\sinh(kh_3)] + \sinh k(h_2 - h_3)[n\rho\omega(iI_3n + \rho\omega) \\ \cosh(kh_1)\cosh(kh_3) + (iI_2n + \rho\omega)^2\sinh(kh_1)\sinh(kh_3)] \end{array} \right]} \quad (A5)$$

$$F_1(y) = \left( \begin{array}{l} f_1 f_2 \sinh[k(h_1 - h_2 - y)] + 2f_3 f_4 \sinh[k(h_1 + h_2 - y)] + \\ f_5 \sinh[k(h_1 + h_2 - 2h_3 - y)] + f_7 \sinh[k(h_1 - h_2 + 2h_3 - y)] + \\ f_9 \sinh[k(h_1 + h_2 + 2h_3 - y)] + f_{11} \sinh[k(h_1 - h_2 + 4h_3 - y)] + \\ f_{13} \sinh[k(h_1 - h_2 + y)] + f_{15} \sinh[k(h_1 + h_2 + y)] + \\ f_{17} \sinh[k(h_1 + h_2 - 4h_3 + y)] + f_{18} \sinh[k(h_1 - h_2 - 2h_3 + y)] + \\ f_{20} \sinh[k(h_1 + h_2 - 2h_3 + y)] + f_{21} \sinh[k(h_1 - h_2 + 2h_3 + y)] \end{array} \right) \quad (\text{A6})$$

$$F_2(y) = \left( \begin{array}{l} f_1 I_2 n^2 \rho \omega \sinh[k(h_1 - h_2 - y)] - 2f_3 I_2 n^2 \rho \omega \sinh[k(h_1 + h_2 - y)] + \\ f_6 \sinh[k(h_1 + h_2 - 2h_3 - y)] + f_8 \sinh[k(h_1 - h_2 + 2h_3 - y)] + \\ f_{10} \sinh[k(h_1 + h_2 + 2h_3 - y)] + f_{12} \sinh[k(h_1 - h_2 + 4h_3 - y)] + \\ f_{14} \sinh[k(h_1 - h_2 + y)] + f_{16} \sinh[k(h_1 + h_2 + y)] - \\ f_{12} \sinh[k(h_1 + h_2 - 4h_3 + y)] + f_{19} \sinh[k(h_1 - h_2 - 2h_3 + y)] - \\ f_8 \sinh[k(h_1 + h_2 - 2h_3 + y)] + f_{22} \sinh[k(h_1 - h_2 + 2h_3 + y)] \end{array} \right) \quad (\text{A7})$$

$$G_1 = \left( \begin{array}{l} g_1 \sinh[k(h_1 - h_2)] + g_3 \sinh[k(h_1 + h_2)] - (I_2 - I_3) n g_5 \\ \sinh[k(h_1 + h_2 - 2h_3)] - (I_2 - I_3) n g_7 \sinh[k(h_1 - h_2 + 2h)] \end{array} \right) \quad (\text{A8})$$

$$G_2 = \left( \begin{array}{l} g_2 \sinh[k(h_1 - h_2)] + g_4 \sinh[k(h_1 + h_2)] - (I_2 - I_3) n g_6 \\ \sinh[k(h_1 + h_2 - 2h_3)] - (I_2 - I_3) n g_8 \sinh[k(h_1 - h_2 + 2h)] \end{array} \right) \quad (\text{A9})$$

$$D_{21} = 2k^2 \left( \begin{array}{l} (2n^2 \rho^2 \omega^2 (I_3^2 n^2 + \rho^2 \omega^2) \cosh[kh_1]^2 \cosh[kh_3]^2 \sinh[k(h_2 - h_3)]^2 + \\ (I_3^2 n^3 \rho^2 \omega^2 + n \rho^4 \omega^4) \cosh[kh_3]^2 \sinh[2kh_1] \sinh[2k(h_2 - h_3)] + \\ (2I_2^4 n^4 + 4I_2^2 n^2 \rho^2 \omega^2 + 2\rho^4 \omega^4) \sinh[kh_1]^2 \sinh[kh_3]^2 \\ \sinh[k(h_2 - h_3)]^2 + (I_2^2 n^3 \rho^2 \omega^2 + n \rho^4 \omega^4) \sinh[2kh_1] \sinh[kh_3]^2 \\ \sinh[2k(h_2 - h_3)] + 2(I_2^2 n^2 + \rho^2 \omega^2) \cosh[k(h_2 - h_3)]^2 \{ (I_3^2 n^2 + \rho^2 \omega^2) \\ \cosh[kh_3]^2 \sinh[kh_1]^2 + n^2 \rho^2 \omega^2 \cosh[kh_1]^2 \sinh[kh_3]^2 \} \end{array} \right) \quad (\text{A10})$$

$$D_{22} = 2k^2 \left( \begin{array}{l} \frac{1}{2} \sinh[2k(h_2 - h_3)] \sinh[2kh_3] \{ 2n \rho^2 \omega^2 (I_2 (I_2 - I_3) n^2 + \\ (I_2 I_3 n^2 + \rho^2 \omega^2) \cosh[2(h_2 - h_3)k] \} \sinh[2kh_1] + (I_2 I_3 n^2 + \rho^2 \omega^2) \\ (-I_2^2 n^2 + (-1 + n^2) \rho^2 \omega^2 + (I_2^2 n^2 + (1 + n^2) \rho^2 \omega^2) \cosh[2kh_1]) \} \end{array} \right) \quad (\text{A11})$$

where

$$f_1 = I_2^2 n^2 + 2I_2 I_3 n^2 + I_3^2 n^2 + 4\rho^2 \omega^2 \quad (\text{A12})$$

$$f_2 = I_2^2 n^2 - (-1+n)\rho^2 \omega^2 \quad (\text{A13})$$

$$f_3 = I_2^2 n^2 + I_3^2 n^2 + 2\rho^2 \omega^2 \quad (\text{A14})$$

$$f_4 = I_2^2 n^2 + (1+n)\rho^2 \omega^2 \quad (\text{A15})$$

$$f_5 = -I_2^4 n^4 + I_2^2 I_3^2 n^4 - (I_2^2 - I_3^2) n^2 \rho^2 \omega^2 - 3I_2^2 n^3 \rho^2 \omega^2 + (2I_2 I_3 + I_3^2) n^3 \rho^2 \omega^2 \quad (\text{A16})$$

$$f_6 = \begin{pmatrix} -2I_2^3 n^3 \rho \omega + 2I_2^2 I_3 n^3 \rho \omega + I_2^3 n^4 \rho \omega - I_3^2 I_2 n^4 \rho \omega - \\ 2(I_2 + I_3) n \rho^3 \omega^3 - 2(I_2 - I_3) n^2 \rho^3 \omega^3 \end{pmatrix} \quad (\text{A17})$$

$$f_7 = -2I_2^4 n^4 + 2I_2^2 I_3^2 n^4 - 2(I_2^2 - I_3^2) n^2 \rho^2 \omega^2 - 2I_2^2 n^3 \rho^2 \omega^2 - 2I_3^2 n^3 \rho^2 \omega^2 \quad (\text{A18})$$

$$f_8 = -2I_2^3 n^4 \rho \omega + 2I_2 I_3^2 n^4 \rho \omega \quad (\text{A19})$$

$$f_9 = -I_2^4 n^4 + I_2^2 I_3^2 n^4 - (I_2^2 - I_3^2) n^2 \rho^2 \omega^2 + I_2^2 n^3 \rho^2 \omega^2 - (2I_2 I_3 - I_3^2) n^3 \rho^2 \omega^2 \quad (\text{A20})$$

$$f_{10} = \begin{pmatrix} 2I_2^3 n^3 \rho \omega - 2I_2^2 I_3 n^3 \rho \omega + I_2^3 n^4 \rho \omega - I_3^2 I_2 n^4 \rho \omega + \\ 2(I_2 - I_3) n \rho^3 \omega^3 + 2(I_2 - I_3) n^2 \rho^3 \omega^3 \end{pmatrix} \quad (\text{A21})$$

$$f_{11} = \begin{pmatrix} I_2^4 n^4 - 2I_2^3 I_3 n^4 + I_2^2 I_3^2 n^4 + (I_2^2 + I_3^2) n^2 \rho^2 \omega^2 - \\ 2I_2 I_3 n^2 \rho^2 \omega^2 - I_2^2 n^3 \rho^2 \omega^2 + (2I_2 I_3 - I_3^2) n^3 \rho^2 \omega^2 \end{pmatrix} \quad (\text{A22})$$

$$f_{12} = (I_2^3 - 2I_2^2 I_3 + I_2 I_3^2) n^4 \rho \omega \quad (\text{A23})$$

$$f_{13} = \left( \begin{array}{l} 2I_2^4 n^4 + 2I_2^2 I_3^2 n^4 + (6I_2^2 + 2I_3^2) n^2 \rho^2 \omega^2 - \\ (2I_2^2 + 2I_3^2) n^3 \rho^2 \omega^2 + 4(1-n) \rho^4 \omega^4 \end{array} \right) \quad (\text{A24})$$

$$f_{14} = (2I_2^3 + 2I_2 I_3^2) n^4 \rho \omega + 4I_2 n^2 \rho^3 \omega^3 \quad (\text{A25})$$

$$f_{15} = \left( \begin{array}{l} I_2^4 n^4 + 2I_2^3 I_3 n^4 + I_2^2 I_3^2 n^4 + (5I_2^2 + 2I_2 I_3 + I_3^2) n^2 \rho^2 \omega^2 + \\ (I_2^2 + 2I_2 I_3 + I_3^2) n^3 \rho^2 \omega^2 + 4(1+n) \rho^4 \omega^4 \end{array} \right) \quad (\text{A26})$$

$$f_{16} = (-I_2^3 - 2I_2^2 I_3 - I_2 I_3^2) n^4 \rho \omega - 4I_2 n^2 \rho^3 \omega^3 \quad (\text{A27})$$

$$f_{17} = \left( \begin{array}{l} I_2^4 n^4 - 2I_2^3 I_3 n^4 + I_2^2 I_3^2 n^4 + (I_2^2 - 2I_2 I_3 + I_3^2) n^2 \rho^2 \omega^2 + \\ (I_2^2 - 2I_2 I_3 + I_3^2) n^3 \rho^2 \omega^2 \end{array} \right) \quad (\text{A28})$$

$$f_{18} = -I_2^4 n^4 + I_2^2 I_3^2 n^4 + (-I_2^2 + I_3^2) n^2 \rho^2 \omega^2 - (I_2^2 - 2I_2 I_3 + I_3^2) n^3 \rho^2 \omega^2 \quad (\text{A29})$$

$$f_{19} = \left( \begin{array}{l} 2I_2^3 n^3 \rho \omega - 2I_2^2 I_3 n^3 \rho \omega - (I_2^3 n^4 - I_3^2 I_2) n^4 \rho \omega + \\ 2(I_2 - I_3) n \rho^3 \omega^3 - 2(I_2 - I_3) n^2 \rho^3 \omega^3 \end{array} \right) \quad (\text{A30})$$

$$f_{20} = -2I_2^4 n^4 + 2I_2^2 I_3^2 n^4 - (2I_2^2 - 2I_3^2) n^2 \rho^2 \omega^2 - (2I_2^2 - 2I_3^2) n^3 \rho^2 \omega^2 \quad (\text{A31})$$

$$f_{21} = -I_2^4 n^4 + I_2^2 I_3^2 n^4 - (I_2^2 - I_3^2) n^2 \rho^2 \omega^2 + (3I_2^2 - 2I_2 I_3 - I_3^2) n^3 \rho^2 \omega^2 \quad (\text{A32})$$

$$f_{22} = \left( \begin{array}{l} -2I_2^3 n^3 \rho \omega + 2I_2^2 I_3 n^3 \rho \omega - (I_2^3 n^4 - I_3^2 I_2) n^4 \rho \omega - \\ 2(I_2 - I_3) n \rho^3 \omega^3 + 2(I_2 - I_3) n^2 \rho^3 \omega^3 \end{array} \right) \quad (\text{A33})$$

$$g_1 = \left( \begin{array}{l} I_2^3 I_3 n^4 + I_2 I_3 n^2 \rho^2 \omega^2 - (-1+n) \rho^2 \omega^2 (I_3^2 n^2 + 2\rho^2 \omega^2) + \\ I_2^2 n^2 (I_3^2 n^2 - (-2+n) \rho^2 \omega^2) \end{array} \right) \quad (\text{A34})$$

$$g_2 = n \rho \omega (I_2^3 n^2 + I_2^2 I_3 (-1+n) n^2 + I_3 (-1+n) \rho^2 \omega^2 + I_2 (I_3^2 n^3 + (1+n) \rho^2 \omega^2)) \quad (\text{A35})$$

$$g_3 = \begin{pmatrix} I_2^3 I_3 n^4 + I_2 I_3 n^2 \rho^2 \omega^2 + (1+n) \rho^2 \omega^2 (I_3^2 n^2 + 2\rho^2 \omega^2) + \\ I_2^2 n^2 (I_3^2 n^2 + (2+n) \rho^2 \omega^2) \end{pmatrix} \quad (\text{A36})$$

$$g_4 = -n \rho \omega (-I_2^3 n^2 + I_2^2 I_3 (1+n) n^2 + I_3 (1+n) \rho^2 \omega^2 + I_2 (I_3^2 n^3 + (-1+n) \rho^2 \omega^2)) \quad (\text{A37})$$

$$g_5 = n (I_2^2 I_3 n^2 + I_2 n \rho^2 \omega^2 + I_3 (1+n) \rho^2 \omega^2) \quad (\text{A38})$$

$$g_6 = \rho \omega (I_2^2 n^2 - I_2 I_3 n^3 + (1+n) \rho^2 \omega^2) \quad (\text{A39})$$

$$g_7 = n (I_2^2 I_3 n^2 - I_2 n \rho^2 \omega^2 - I_3 (-1+n) \rho^2 \omega^2) \quad (\text{A40})$$

$$g_8 = \rho \omega (I_2^2 n^2 + I_2 I_3 n^3 - (-1+n) \rho^2 \omega^2) \quad (\text{A41})$$

### Discharge Velocities

$$S_1(y) = \begin{pmatrix} f_1 f_2 \cosh[k(h_1 - h_2 - y)] + 2f_3 f_4 \cosh[k(h_1 + h_2 - y)] + \\ f_5 \cosh[k(h_1 + h_2 - 2h_3 - y)] + f_7 \cosh[k(h_1 - h_2 + 2h_3 - y)] + \\ f_9 \cosh[k(h_1 + h_2 + 2h_3 - y)] + f_{11} \cosh[k(h_1 - h_2 + 4h_3 - y)] - \\ f_{13} \cosh[k(h_1 - h_2 + y)] - f_{15} \cosh[k(h_1 + h_2 + y)] - \\ f_{17} \cosh[k(h_1 + h_2 - 4h_3 + y)] - f_{18} \cosh[k(h_1 - h_2 - 2h_3 + y)] - \\ f_{20} \cosh[k(h_1 + h_2 - 2h_3 + y)] - f_{21} \cosh[k(h_1 - h_2 + 2h_3 + y)] \end{pmatrix} \quad (\text{A42})$$

$$S_2(y) = \begin{pmatrix} f_1 I_2 n^2 \rho \omega \cosh[k(h_1 - h_2 - y)] - 2f_3 I_2 n^2 \rho \omega \cosh[k(h_1 + h_2 - y)] + \\ f_6 \cosh[k(h_1 + h_2 - 2h_3 - y)] + f_8 \cosh[k(h_1 - h_2 + 2h_3 - y)] + \\ f_{10} \cosh[k(h_1 + h_2 + 2h_3 - y)] + f_{12} \cosh[k(h_1 - h_2 + 4h_3 - y)] - \\ f_{14} \cosh[k(h_1 - h_2 + y)] - f_{16} \cosh[k(h_1 + h_2 + y)] + \\ f_{12} \cosh[k(h_1 + h_2 - 4h_3 + y)] - f_{19} \cosh[k(h_1 - h_2 - 2h_3 + y)] + \\ f_8 \cosh[k(h_1 + h_2 - 2h_3 + y)] - f_{22} \cosh[k(h_1 - h_2 + 2h_3 + y)] \end{pmatrix} \quad (\text{A43})$$

## Acknowledgments

The first author thanks Professor Cesar Mendoza for originally suggesting this subject of study and acknowledges the support of the *Boris A. Bakhmeteff* Research Fellowship at Columbia University. The authors acknowledge the thorough and constructive reviews provide by two anonymous reviewers and the editor's office.

## References

Bagtzoglou, A. C., A. F. B. Tompson, and D. E. Dougherty, Probabilistic simulation for reliable solute source identification in heterogeneous porous media, *Water Resources Engineering Risk Assessment*, NATO ASI Series, Vol. G 29, Springer-Verlag Berlin Heidelberg, 1991.

Bagtzoglou, A.C., A.F.B. Tompson, and D.E. Dougherty, Projection Functions for Particle-Grid Methods, *Numerical Methods for Partial Differential Equations*, 8, p.325-340, 1992.

Bencala, K. E., Simulation of solute transport in a mountain pool-and-riffle stream with a kinetic mass transfer model for sorption, *Water Resour. Res.*, 19(3), 732-738, 1983.

Bencala, K. E., and R. A. Walters, Simulation of solute transport in a mountain pool-and-riffle stream: A transient storage model, *Water Resour. Res.*, 19(3), 718-724, 1983.

Elliott, A. H., and N. H. Brooks, Transfer of nonsorbing solutes to a streambed with bed forms: Theory, *Water Resour. Res.*, 33(1), 123-136, 1997a.

Elliott, A. H., and N. H. Brooks, Transfer of nonsorbing solutes to a streambed with bed forms: Laboratory experiments, *Water Resour. Res.*, 33(1), 137-151, 1997b.

Gu, Z., and H. Wang, Gravity waves over porous bottoms, *Coastal Engineering*, 15, 497-524, 1991.

Harrison, W. D., D. Musgrave, and W. S. Reeburgh, A wave-induced transport process in marine sediments, *J. of Geophys. Res.*, 88(C12), 7617-7622, 1983.

Huettel, M., W. Ziebis, and S. Forster, Flow-induced uptake of particulate matter in permeable sediments, *Limnol. Oceanogr.*, 41(2), 309-332, 1996.

Iwasa, Y., and S. Aya, Mass transport in the flow over permeable boundaries, *AIHR Congress*, 263-268, 1987.

Joseph, D. D., D. A. Nield, and G. Papanicolaou, Nonlinear equation governing flow in a saturated porous medium, *Water Resour. Res.*, 18(4), 1049-1052, 1982.

Lamb, H., *Hydrodynamics*, Dover Publication, New York, Sixth edition, 1932.

Mendoza, C., Comment on "Convective transport within stable river sediments" by S. A. Savant, D. D. Reible, and L. J. Thibodeaux, *Water Resour. Res.*, 24(7), 1206-1207, 1988.

Murray, J. D., Viscous damping of gravity waves over a permeable bed, *J. of Geophys. Res.*, 70(10), 1965.

Musgrave, D. L., and W. S. Reeburgh, Density-driven interstitial water motion in sediments, *Nature*, 299(5881), 331-334, 1982

Packman, A. I., N. H. Brooks, and J. J. Morgan, A physicochemical model for colloid exchange between a stream and a sand streambed with bed forms, *Water Resour. Res.*, 36(8), 2351-2361, 2000a.

Packman, A. I., N. H. Brooks, and J. J. Morgan, Kaolinite exchange between a stream and streambed: Laboratory experiments and validation of a colloid transport model, *Water Resour. Res.*, 36(8), 2363-2372, 2000b.

Riedl, R. J., N. Huang, and R. Machan, The subtidal pump: A mechanism of interstitial water exchange by wave action, *Mar. Biol.*, 13(3), 210-221, 1972.

Runkel, R. L., K. E. Bencala, R. E. Broshears, and S. C. Chapra, Reactive solute transport in streams, 1. Development of an equilibrium-based model, *Water Resour. Res.*, 32(2), 409-418, 1996.

Savant, A.S. D. O. Reible, and L. J. Thibodeaux, Convective transport within stable river sediments, *Water Resour. Res.*, 23(9), 1763-1768, 1987.

Shum K. T., Wave-induced advective transport below a rippled water-sediment interface, *Water Resour. Res.*, 97(C1), 789-808, 1992.

Tenenbaum, M., and H. Pollard, *Ordinary Differential Equations*, Dover Publications, New York, 1985.

---

Wave period, $T$	10 s
Time, $t$	5 s
Sediment thickness, $h_2$	2 m
Mean water depth, $h_1$	2 m
Wavelength, $\chi$	5 m
Wave amplitude, $E$	1 m
Porosity, $n$	0.25
Water density, $\rho$	1000 kg/m <sup>3</sup>
Permeability, $K$	$5 \times 10^{-11}$ m <sup>2</sup>
Dynamic viscosity, $\mu$	0.001 kg/m s

---

Table 1. Parameters used for the analytical comparison.

---

Wave period, $T$	10 s
Time, $t$	5 s
Sediment thickness, $h_2$	2 m
Thickness of the boundary layer, $h_2 - h_3$	0.2 m (base case) 0 to 1 m
Mean water depth, $h_1$	2 m
Wavelength, $\chi$	5 m
Wave amplitude, $E$	1 m
Porosity, $n$	0.25
Water density, $\rho$	1000 kg/m <sup>3</sup>
Permeability, $K$	5 × 10 <sup>-11</sup> m <sup>2</sup> (base case) 1 × 10 <sup>-11</sup> to 1 × 10 <sup>-10</sup> m <sup>2</sup>
Dynamic viscosity, $\mu$	0.001 kg/m s
Constant $c$	0.6

---

Table 2. Parameters used for the sensitivity analysis.

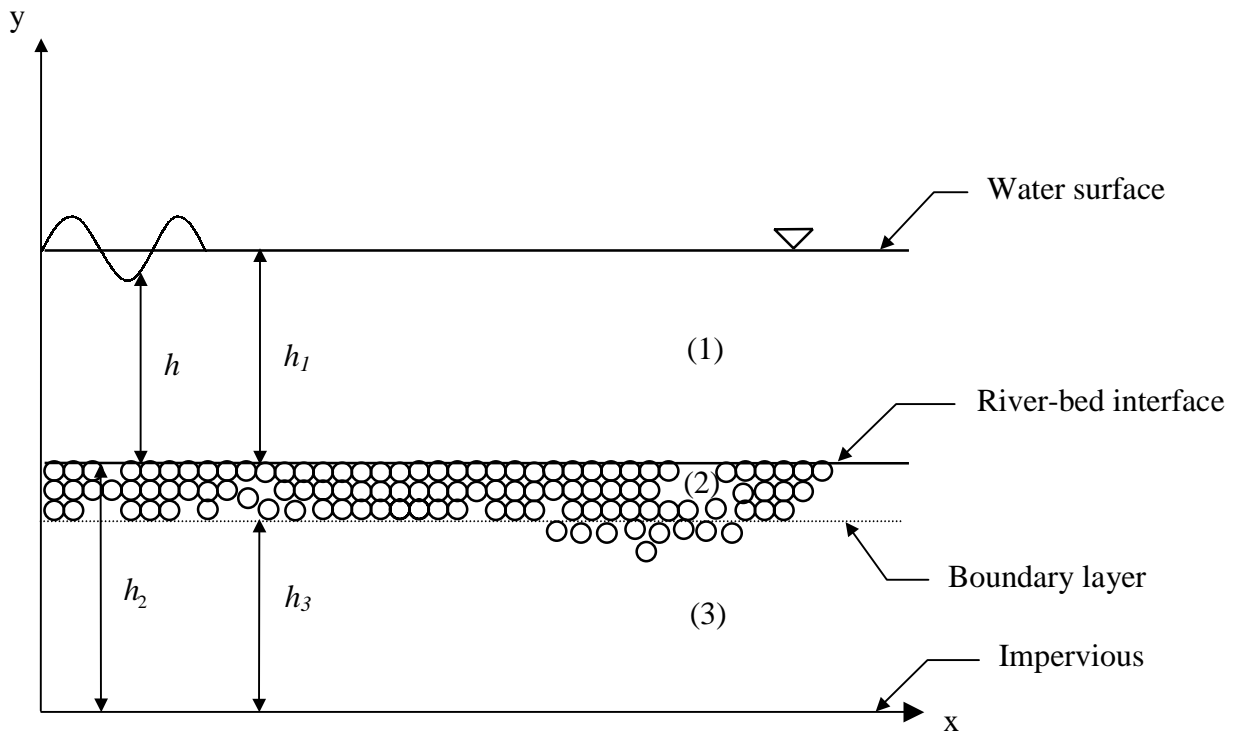


Figure1. A sketch of the physical domain

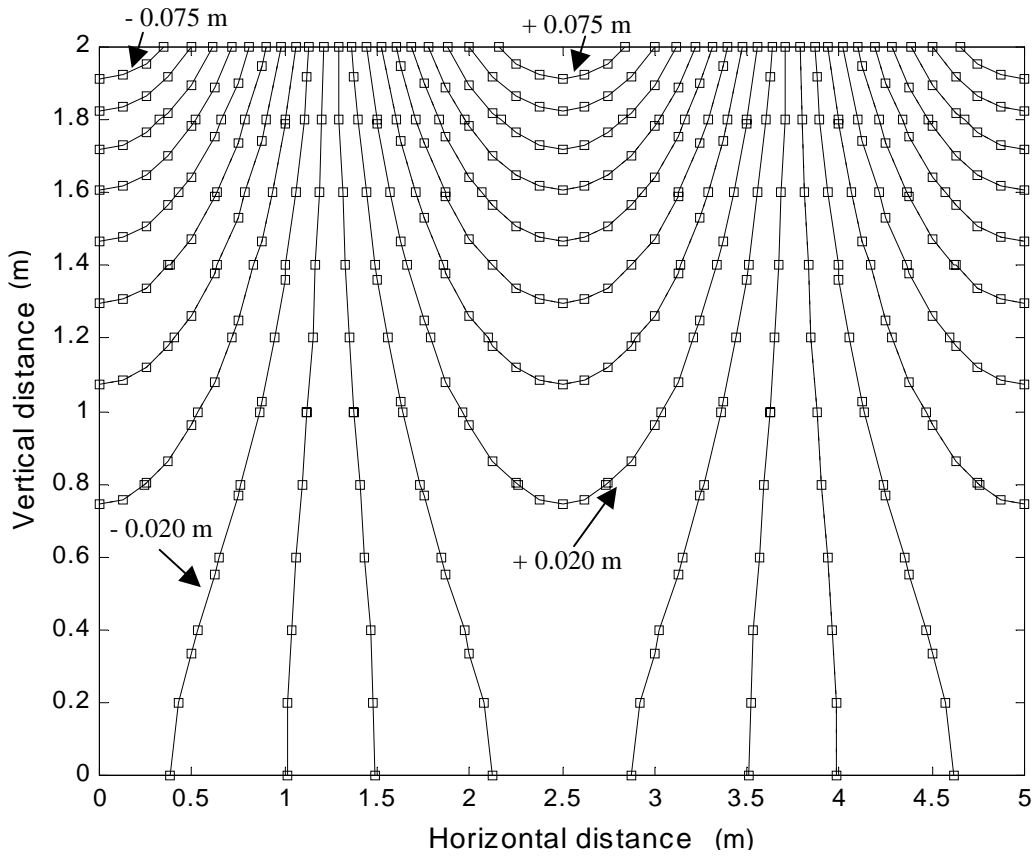


Figure 2. Comparison between equation 30 (solid lines) and the analytical pressure head solution of *Gu and Wang* [1991] (squares). The input parameters used in the comparison are listed in Table 1.

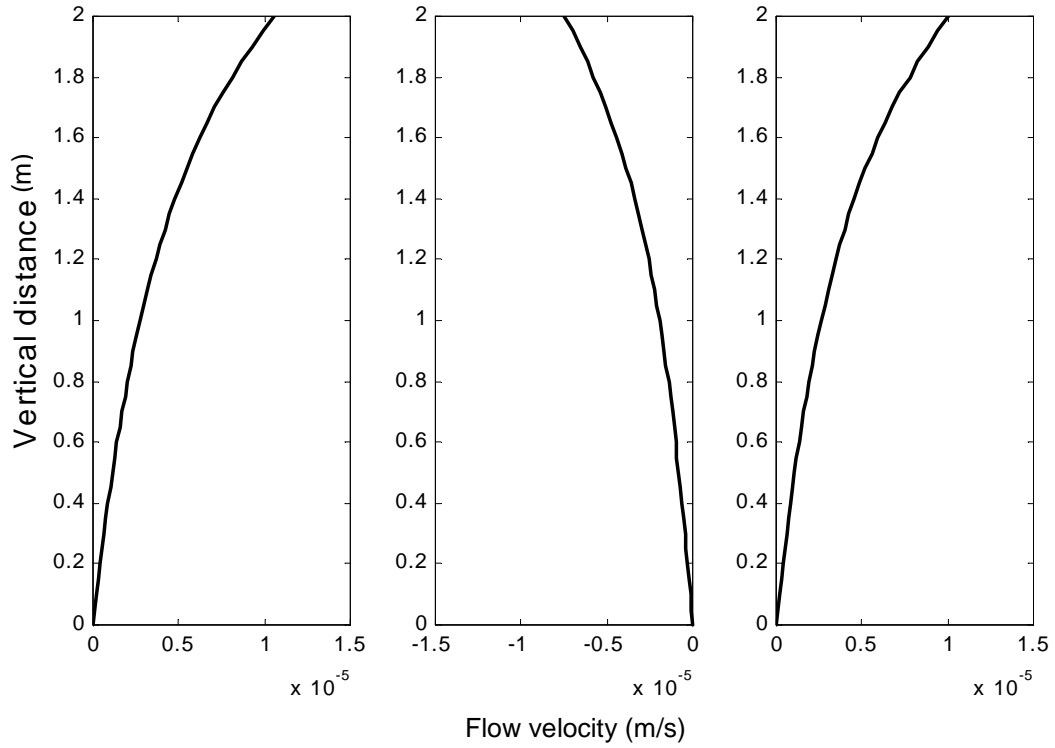


Figure 3. Vertical velocity underneath the water wave. The first plot is measured at the beginning of the water wave, the second in the middle, and the third just before the end of the water wave. Negative values of velocity refer to downward flow.

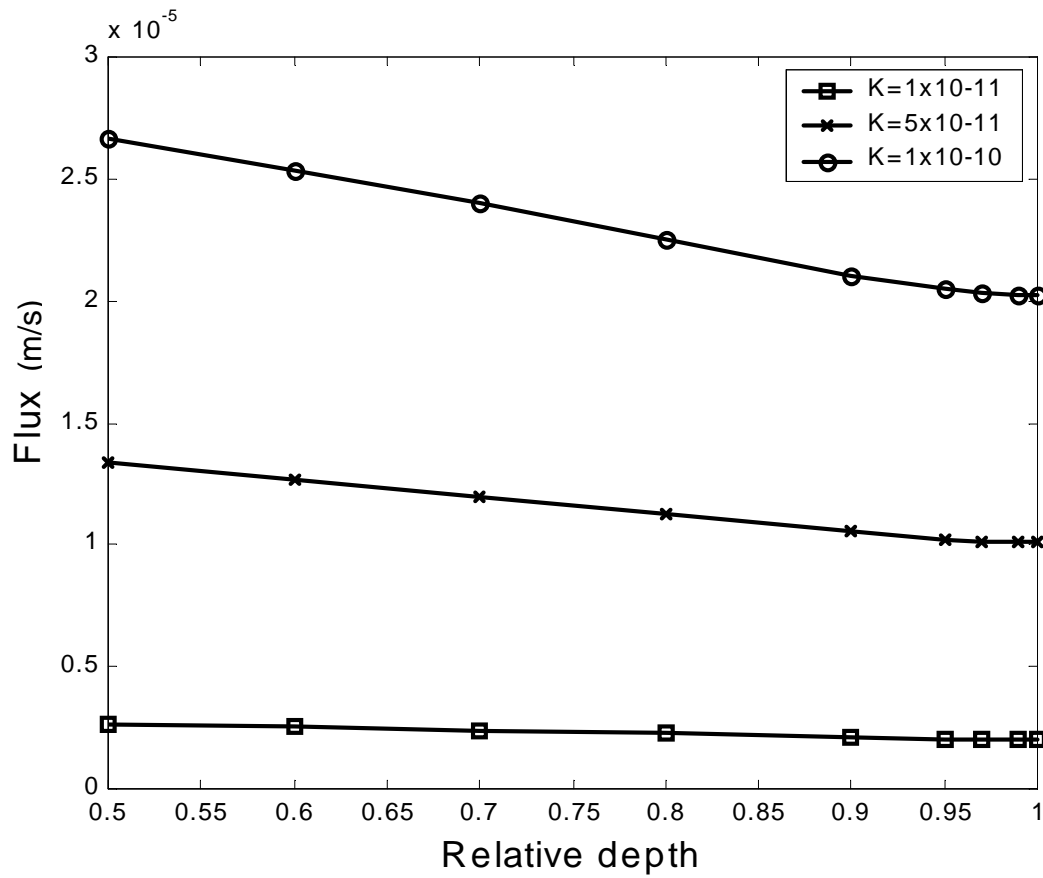


Figure 4. Variation of the unit flux across the riverbed interface with the ratio of the boundary layer's thickness to the total sediment thickness,  $R$ , as a function of three different permeability values (in  $m^2$ ). The flux is averaged over one wave period.

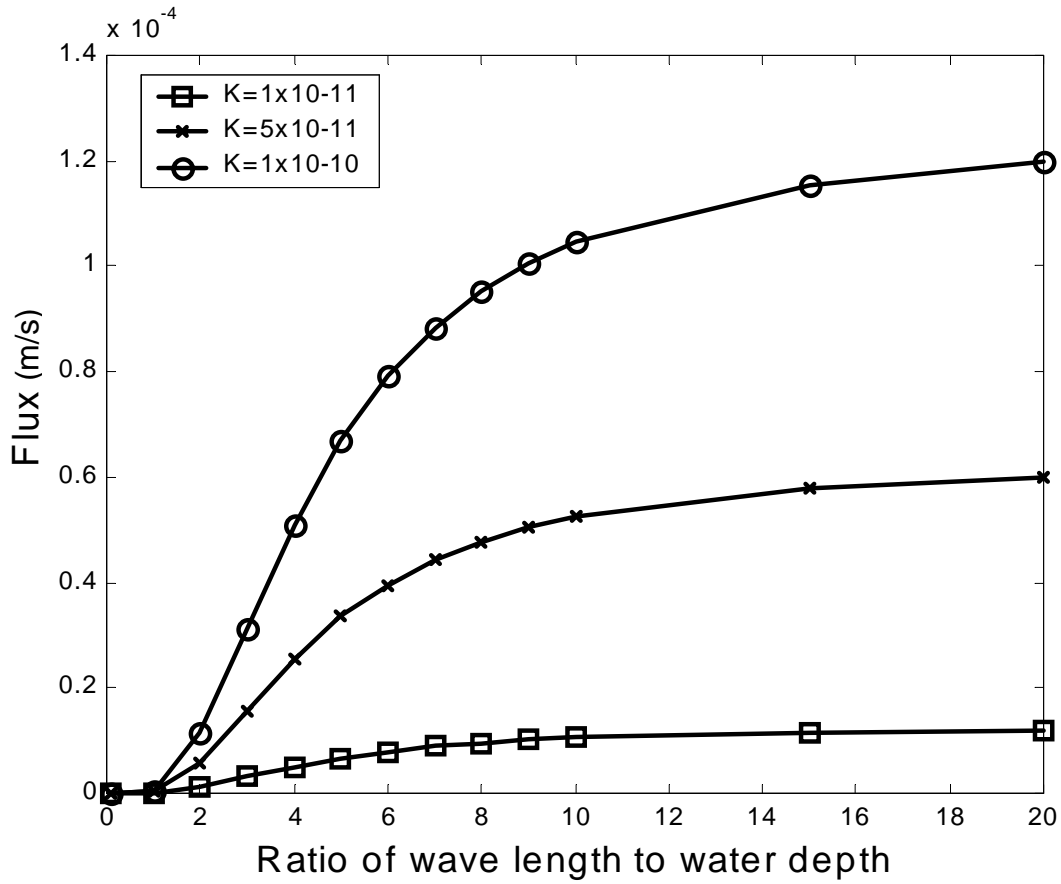


Figure 5. Variation of the unit flux across the riverbed interface with  $S$ , the ratio of the wavelength to the depth of the water channel as a function of three different permeability values (in  $m^2$ ). The flux is averaged over one wave period. The input parameters used in this sensitivity analysis are listed in Table 2.

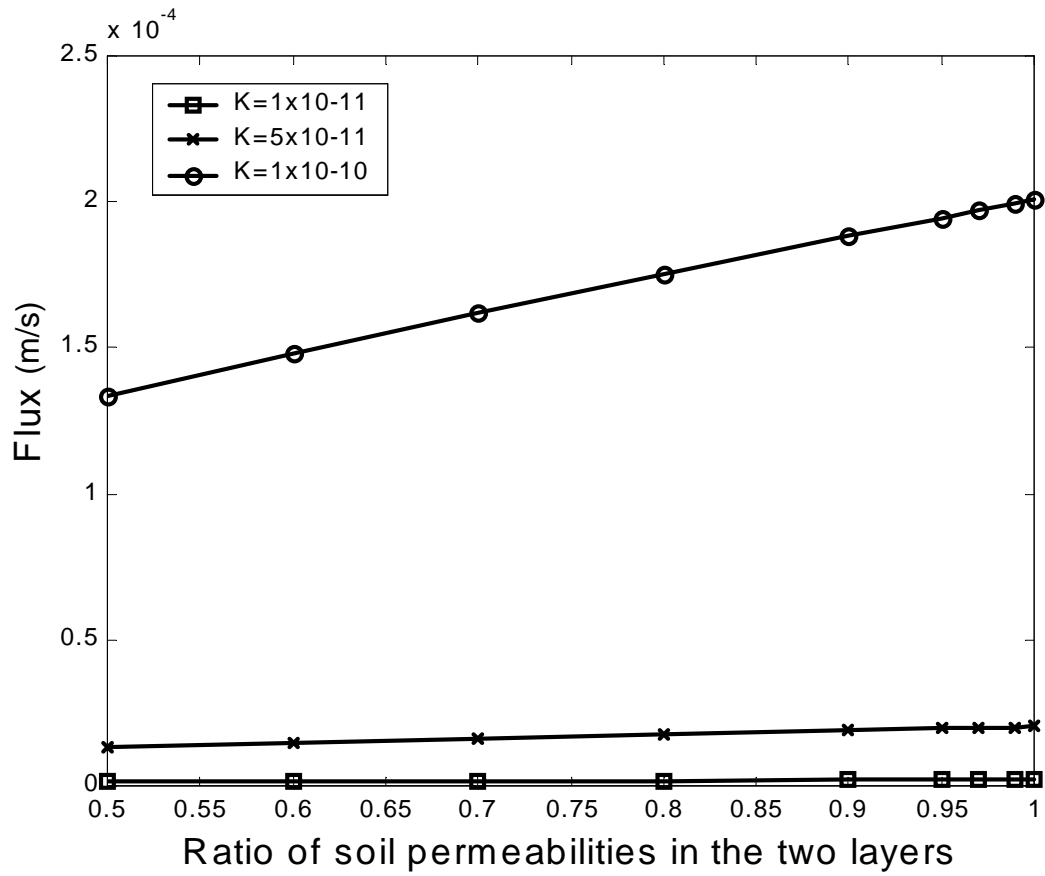


Figure 6. Variation of the unit flux across the riverbed interface with the ratio of the boundary layer's permeability to the sediment's permeability  $K_2/K_3$  as a function of three different permeability values (in  $m^2$ ).

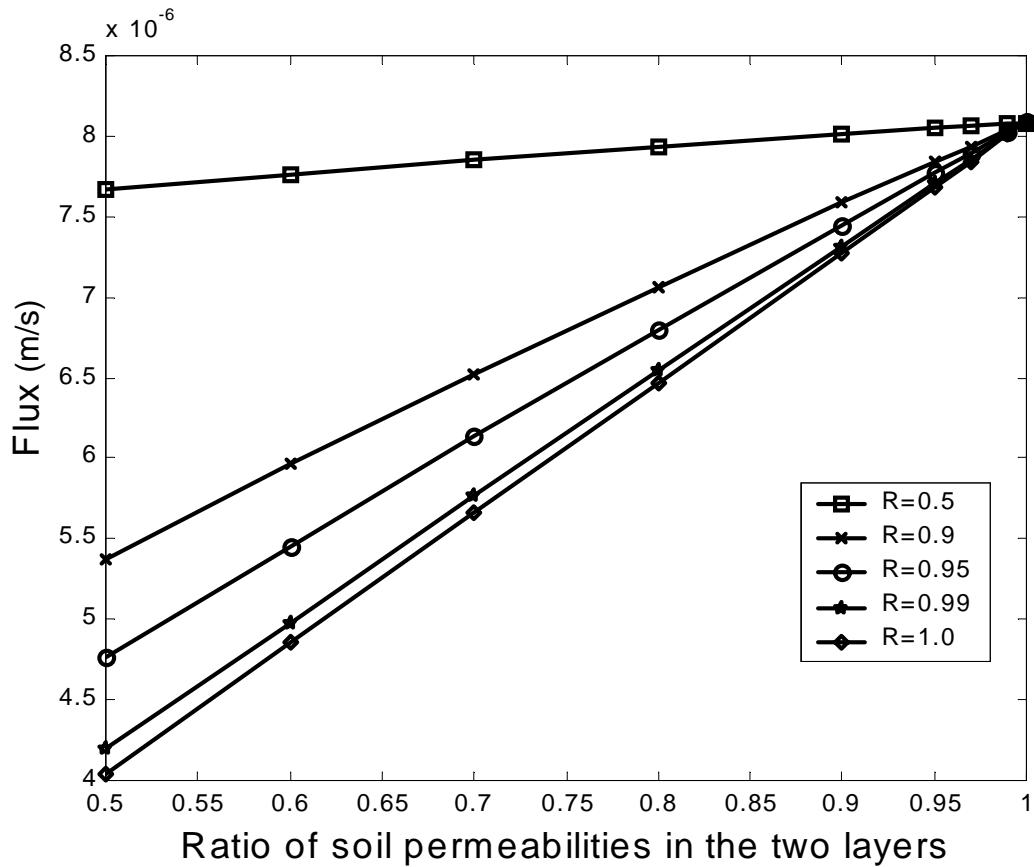
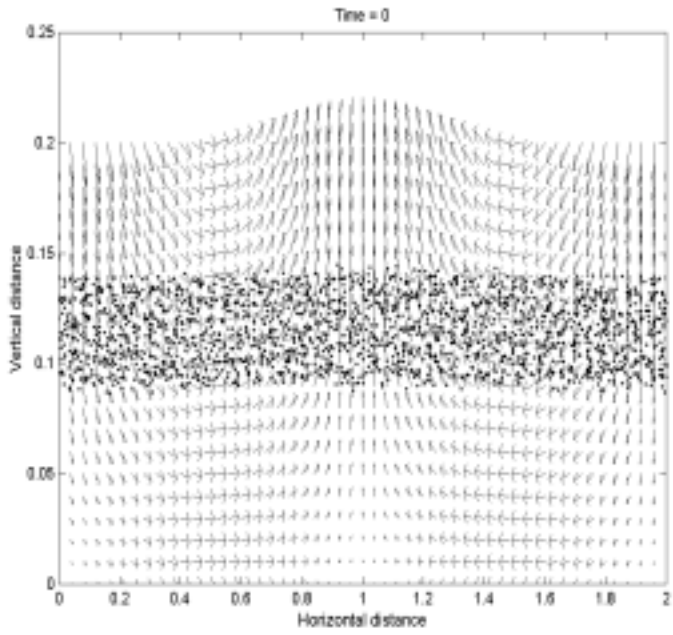
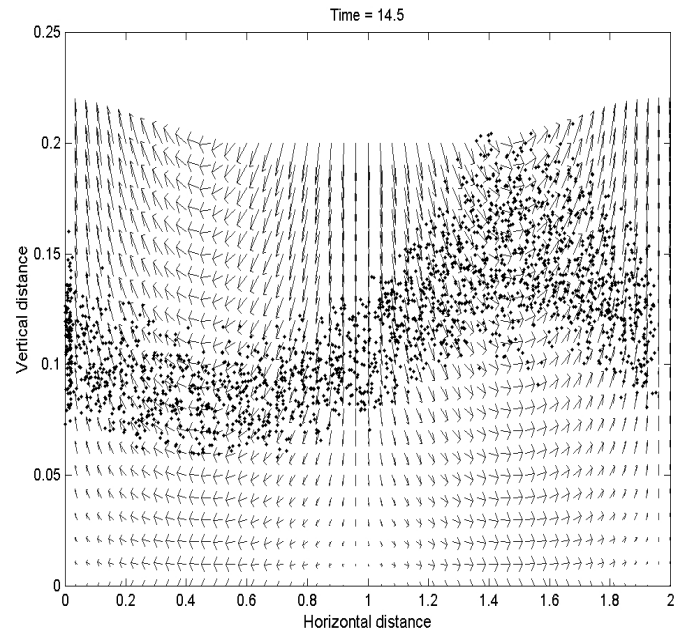


Figure 7. Variation of the unit flux across the riverbed interface with the ratio of the boundary layer's permeability to the sediment's permeability  $K_2/K_3$  as a function of the boundary layer's relative thickness. Note that the value  $R=1$  can never be reached physically and is presented in order to delineate an asymptotically approximated envelope.



a)



b)

Figure 8. Random walk transport simulation results with transport velocity fields obtained from the model presented in this work. a) Initial tracer condition, b) tracer particles at  $t=14.5$  sec.

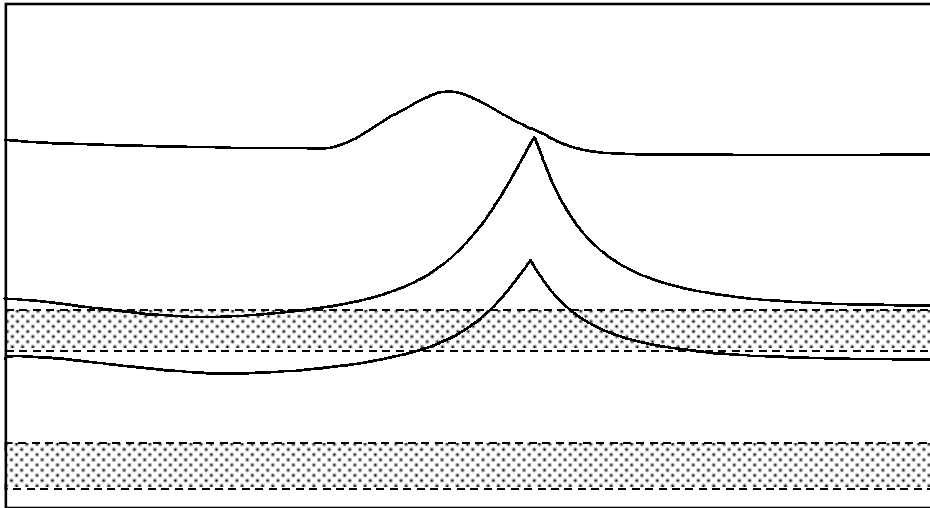


Figure 9. Adaptation of the experimental results of *Huettel et al.* [1996, Experiment 2], showing the distribution of solutes (thin dark lines) in a permeable bed being initially placed in two horizontal layers (hatched zones). Note that only the top solute layer has exhibited any noticeable changes.